Published in final edited form as:
Acad Radiol. 2011 September ; 18(9): 1123–1132. doi:10.1016/j.acra.2011.04.012.

Acoustic Droplet Vaporization for Enhancement of Thermal Ablation by High Intensity Focused Ultrasound

Man Zhang, MD, PhD[1], **Mario L. Fabiilli, PhD**[1], **Kevin J. Haworth, PhD**[1], **Frederic Padilla, PhD**[1,2], **Scott D. Swanson, PhD**[1], **Oliver D. Kripfgans, PhD**[1], **Paul L. Carson, PhD**[1], and **J. Brian Fowlkes, PhD**[1]

[1]Department of Radiology, University of Michigan Health System, 1301 Catherine Street, Ann Arbor, MI 48109

[2]UMR CNRS 7623, Laboratoire d'Imagerie Parametrique, Paris, France

Abstract

Rationale and Objectives—Acoustic droplet vaporization (ADV) shows promise for spatial control and acceleration of thermal lesion production. Our hypothesis was that microbubbles generated by ADV could enhance high intensity focused ultrasound (HIFU) thermal ablation by controlling and increasing local energy absorption.

Materials and Methods—Thermal lesions were produced in tissue-mimicking phantoms using focused ultrasound (1.44 MHz) with a focal intensity of 4000 $W \cdot cm^{-2}$ in degassed water at 37°C. The average lesion volume was measured by visible change in optical opacity and by T_2-weighted MRI. In addition, *in vivo* HIFU lesions were generated in a canine liver before and after an intravenous injection of droplets with a similar acoustic setup.

Results—Thermal lesions were seven-fold larger in phantoms containing droplets (3×10^5 droplets/mL) compared to phantoms without droplets. The mean lesion volume with a 2 s HIFU exposure in droplet-containing phantoms was comparable to that made by a 5 s exposure in phantoms without droplets. In the *in vivo* study, the average lesion volumes without and with droplets were 0.017 ± 0.006 cm^3 (n = 4, 5 s exposure) and 0.265 ± 0.005 cm^3 (n = 3, 5 s exposure), respectively – a factor of 15 difference. The shape of ADV bubbles imaged with B-mode ultrasound was very similar to the actual lesion shape as measured optically and by MRI.

Conclusion—ADV bubbles may facilitate *clinical* HIFU ablation by reducing treatment time or requisite *in situ* total acoustic power, and provide ultrasonic imaging feedback of the thermal therapy.

Keywords

minimally invasive therapy; microbubble; thermal lesion size; ultrasound; *in vivo*

Introduction

Each year, over 500,000 new cases of liver cancer are diagnosed worldwide and the incidence is continuously increasing in the United States (1). Although surgical resection and liver transplantation are curative (2), only 20% – 30% of the patients are suitable for surgery due to contraindications and limited number of donors (3). Overall, the five-year

Corresponding Author: Man Zhang, M.D., Ph.D., Department of Radiology, University of Michigan Health System, 3232 Medical Sciences Building I, 1301 Catherine Street, Ann Arbor, MI 48109-5667, Tel: (734) 615-0152, Fax: (734) 764-8541, maggiez@umich.edu.

survival rates of liver cancer are less than 10% (4). For these reasons, minimally invasive thermal therapies including radio frequency ablation and high intensity focused ultrasound (HIFU) have been developed and are currently being used or evaluated for treatment of liver masses. HIFU therapy is a non-invasive technique wherein focused ultrasound beams are emitted from a high-powered transducer to thermally ablate a tissue volume inside the body. HIFU systems commonly operate in a frequency range of 1 – 5 MHz, generating high focal intensities up to 30 $kW \cdot cm^{-2}$. Such intensities can increase the tissue temperature beyond 60 °C within the focal volume in seconds, resulting in irreversible protein denaturation, cell destruction, and associated coagulative necrosis (5). Two principal mechanisms, direct absorption of the transmitted pressure wave and acoustic cavitation, may cause tissue heating synergistically (6). The initial applications of HIFU on biological tissues were proposed by Lynn *et al.* (7). Later, Burov (8) suggested using HIFU to treat malignant tumors. The bioeffects and specific properties of focused ultrasound on tissues have been investigated in further studies (9-12) and the physical principles associated with HIFU are becoming better understood (13).

HIFU treatment has distinct advantages over other focal ablative therapies. It is noninvasive and nonionizing. The focused energy is sufficient to induce thermal coagulation in a small volume within seconds, therefore, the blood perfusion effects are minimized (14). However, a major difficulty has been creating homogenous, reproducible, and uniformly shaped lesions (15) and producing these in such a manner as to treat large volumes at a rate that does not damage overlying tissues but achieves full treatment in a clinically manageable time period.

Over the past decade, studies have been performed to demonstrate that acoustic cavitation may be used as a method to enhance HIFU and to overcome the above-mentioned issues (16-18). Historically, bubbles were recognized as a complicating factor for HIFU due to shadowing, lack of control over bubble dynamics, and the induced migration of thermal lesions towards the transducer. These problems have begun to be mitigated more recently by techniques that help control microbubble nucleation and cavitation dynamics and monitoring (6, 19, 20). Significant work has also been done to better understand the effects of bubbles on HIFU lesion formation (16, 18, 19, 21-23).

Several studies have shown that the thermal contribution of microbubbles can be very significant. Ultrasound contrast agent (UCA) has been reported (24) to facilitate HIFU treatment by this manner. For a 100 kPa increase in transmitted pressure, bubble-enhanced HIFU can achieve a 500% or greater temperature increase, whereas without bubbles, only a 20% increase is observed (6). At a UCA concentration of 0.001% and 29 W of ultrasound, a lesion twelve-fold larger was produced than without UCA in tissue mimicking phantoms (25). However, it was observed that UCA moved the greatest heating position from the expected focus by as much as 2 cm for UCA concentrations greater than 0.1%. Some inertial cavitation damage occurred in tissues well outside the thermal lesion (25). Therefore, additional approaches that demonstrate further control over lesion formation may be advantageous.

Acoustic droplet vaporization (ADV) is an ultrasound method for converting biocompatible microdroplets into microbubbles (26-28). When transpulmonary perfluorocarbon droplets are insonified with pressure amplitudes above a threshold value, the droplets phase transition into gas bubbles approximately 5-6 times larger in diameter (29). If the pressure amplitude exceeds the ADV threshold only at the focus, then microbubbles are produced at the focus and can result in a local increase in the acoustic absorption. Thus the increased heating with ADV can be limited to the focus allowing for lower source intensities and/or shorter treatment times. Increased absorption by bubbles at the focus, on the other hand, reduces

risk to distal tissues by decreasing the transmitted acoustic energy (30). ADV bubbles are stable for several minutes or longer and can cause vascular occlusion when lodged in a capillary or other small vessels (26, 31), which is favorable for the HIFU therapy. These microbubbles are highly echogenic *in vivo* (31, 32) for real-time ultrasound imaging. Therefore, the ultrasonic monitoring of HIFU when microbubbles are created during the ADV process may offer opportunities to visualize the treatment process earlier in the lesion formation.

Preliminary *in vitro* evaluation of ADV for HIFU enhancement was performed with a phase-shift nanoemulsion (33). There it was found that the nanoemulsion may provide spatial and temporal control of bubble-enhanced heating. In this study, we investigated the hypothesis that ADV bubbles from micrometer-sized droplets generated in an appropriate density substantially enhance HIFU ablative therapy by increasing thermal lesion volume or equivalently shortening the treatment time as compared to traditional non-bubble based HIFU. A second hypothesis that ADV microbubbles could be used for image-guided feedback of the HIFU lesion location, size, and shape was also tested. Experiments were performed in both tissue-mimicking phantoms and in canine liver *in vivo*.

Materials and Methods

A. Perfluoropentane Droplet Preparation

Lipid coated perfluoropentane droplets were made according to a previously described protocol (34) and stored in the refrigerator (5°C) for up to four weeks. Prior to use, the droplet size distribution and number density was obtained with a Coulter counter (Multisizer 3, Beckman Coulter Inc., Fullerton, CA) The mean diameter of the droplets was 2.0 ± 0.1 μm with ~99% of droplets smaller than 8 μm (Figure 1).

B. Tissue-mimicking phantom study

HIFU/ADV phantoms were fabricated based on previously described methods (35). The tissue-mimicking phantoms consisted of 33% (v/v) of an aqueous acrylamide solution (30% w/v, Sigma-Aldrich, St. Louis, MO), 31.4% (v/v) of degassed deionized water, 35% (v/v) of egg white, 0.5% (v/v) of 10% ammonium persulfate (A3678, Sigma-Aldrich), 0.1% (v/v) tetramethylethylenediamine (T8133, Sigma-Aldrich) and various concentrations of perfluoropentane droplets. During phantom preparation, the gel solution was degassed before the addition of droplets to minimize spurious gas inclusions that might act as cavitation nuclei. These egg white-based phantoms were optically transparent. If HIFU increased the temperature in a portion of the phantom to > 60°C, the egg white protein would denature and coagulate, resulting in a permanently opaque, optically observable lesion. The acoustic attenuation of these phantoms was approximately 0.3 dB/cm (35) at 1.44 MHz.

The HIFU therapy system consisted of a high power spherical section transducer (63.5 mm diameter, f-number = 1, Etalon 940501, Lebanon, IN, USA) driven with an ENI A300 amplifier (ENI Inc., Rochester, NY, USA) at 1.44 MHz. A function generator (3314A, Agilent, Palo Alto, CA, USA) was gated with a secondary function generator (33120A, Agilent) to produce the continuous wave (CW) feeding signals to the amplifier for ultrasound exposures with durations of 2 to 5 s. The lateral beam width and axial depth of field at the focus (full-width, half maximum intensity) were 1.6 mm and 8.2 mm, respectively. A needle-type thermocouple (300 μm diameter, Omega, Stamford, CT, USA) was inserted orthogonally to the acoustic beam path and 2 mm away from the transducer focus through a guide in the side of the phantom. A data logger (TC-08, Pico Technology, Cambridge, UK) was used to record the temperature change. The experimental setup is

shown in Figure 2. The therapy transducer was calibrated using a membrane hydrophone (ST223, Sonic Industries, Hatboro, PA, USA) in degassed water at room temperature, and the output waveforms from the hydrophone were captured by an oscilloscope (9314L, LeCroy Corp., Chestnut Ridge, NY, USA). A peak rarefactional pressure of 7.4 MPa and a peak positive pressure of 17.7 MPa were measured at the focus. A focal intensity of 4000 $W \cdot cm^{-2}$ was then estimated from the measured waveforms (Figure 3).

C. *In vivo* HIFU in canine liver

1. Animal preparation—A canine model was chosen because its liver size is of human scale and canines display a similar tolerance for perfluorocarbon emulsions as humans (36). The canine was initially sedated by an intramuscular injection of acepromazine followed by sodium thiopental for the induction of anesthesia. The canine was then intubated and full anesthesia maintained by inhalation of isoflurane. Following induction of anesthesia, heart rate, blood oxygenation, body temperature, and respiratory rate were monitored. The liver was targeted for HIFU ablation with the animal in a dorsal recumbency position. A laparotomy was performed to expose the liver. A 37 °C degassed water bath was coupled to the externalized liver covered with a layer of degassed ultrasound gel – water mixture (1:1 mix ratio) to provide an acoustic path and maintain an appropriate body temperature. All procedures were approved by the University Committee on Use and Care of Animals.

2. HIFU lesion generation—The same HIFU transducer from the *in vitro* studies (1.44 MHz) was mounted on a 3D micropositioning system (Parker-Hannifin Corp., Cleveland, OH, USA) and used to produce thermal lesions in the liver. A focal pointer was used to identify the acoustic beam path and determine the focal spot. Best efforts were made to ensure that the therapeutic acoustic path was oriented perpendicular to the liver surface. The tip of the pointer barely touched the anterior surface of the liver. The transducer position was recorded by the 3D micropositioning system. The pointer was then removed and the focus of the HIFU transducer was set 15 mm below the liver surface. An ultrasound imager (4D 16L, GE Ultrasound) was used to ensure that no major vessels were within the therapeutic beam path and to image the ADV bubble cloud.

The acoustic parameters used for *in vivo* HIFU ablation were similar to those for the phantom study. The exposure duration was either 3 s or 5 s. Prior to the intravenous (IV) injection of droplets, 3 s lesions (n = 4) were generated in a row with 10 mm spacing on the caudal side of the liver. B-mode ultrasound was used immediately after to image these lesions. The HIFU transducer was then moved 10 mm towards the cranial side so that thermal lesions with 5 s exposure (n = 4) were produced and then imaged. In each row, the lesions were produced in an alternating manner – with a 3 s interval between each lesion - such that two adjacent lesions were not produced sequentially. Therefore, the previously made lesion had minimal thermal effect on the subsequent lesion. During the thermal lesion production, the canine was placed on a ventilator and 35 s breathing pauses were employed to reduce tissue motion.

For IV droplet injections, a 23 Fr butterfly catheter (Becton Dickinson, Franklin Lakes, NJ, USA) was placed in the cephalic vein. The injection dose, consisting of 6 mL of droplet preparation injected over 1 minute, was 1×10^8 droplets/kg. The droplet number density in tissue was similar to the recommended Definity® UCA (Lantheus Medical Imaging, N. Billerica, MA) dosage of 1.2×10^8 microbubbles/kg. However, the effective perfluorocarbon dose is larger, compared to UCA, since the droplets contain liquid (i.e. more dense) perfluorocarbon. During the droplet injection, a linear imager (10L GE Ultrasound, Milwaukee, WI) with an MI of 0.9 was targeted to a smaller liver lobe. The sparse ADV microbubbles generated by the imaging array were observed on the B-mode image,

indicating the presence of droplets in the liver. Subsequently, two groups of thermal lesions were produced with either a 3 s (n = 4) or 5 s (n = 4) exposure. The procedure, except for the injection of droplets, was identical to that used for lesions without the droplets. The spacing between neighboring lesions was 15 mm to prevent overlap of adjacent lesions. A third set of HIFU lesions (n = 4) with 5 s exposure were made 30 min after the droplet injection and again imaged with ultrasound. Then the animal was euthanized and the liver was harvested two hours later to allow the acute thermal effects to develop.

D. Lesion size estimation using ultrasound, visible macroscopic imaging, and MRI

The volume and shape of thermal lesions were assessed by two methods – visible opacity change and MRI measurements. The bubble-lesion size and shape imaged by ultrasound were compared to the visual and MRI estimation of these lesions.

In both *in vitro* and *in vivo* experiments, a linear imaging array (10L, Logiq 9, GE Ultrasound, Milwaukee, WI, USA) was used to image the ADV microbubble formation immediately after the HIFU process. The acoustic output of the imager (displayed MI = 0.35) was set below the ADV threshold in order to avoid vaporizing droplets with the imager. Then, specimens were measured by MRI. Here, the transverse magnetization relaxation time constant, T_2, is sensitive to slow molecular motions of water. The denatured and cross-linked proteins caused a significant decrease in the water proton mobility and thereby a decrease in the water proton T_2 (37), which was observed as a darker region in Figure 4. Therefore, MRI provided an alternative, independent, and direct method of measuring protein coagulation (38), and was utilized to verify the uniformity of these *in vitro* and *in vivo* thermal lesions. The spin-echo MRI imaging sequence with T_2 weighting was performed within 30 min after thermal lesion production in the phantoms or liver harvesting. MRI lesion volumes were measured with ImageJ software (National Institutes of Health, Bethesda, MD, USA) in each acquired image slice using a binary threshold. A high contrast between the mean gray levels inside the lesions and the surrounding background was observed. The mean gray levels were separated by at least nine standard deviations for the *in vitro* phantom data, and by four standard deviations for the *in vivo* liver images. The standard deviations were found to be similar in the lesion and in the background medium, approximately 5% of the mean value. Therefore, a simple thresholding was applied in each section to discriminate pixels included in the lesions from pixels of the background, with a threshold set to the mid-value between the mean gray level values in the lesion and in the background. Finally, the visible volumes of the lesions were measured. Lesions were dissected based on the color change, and their volume was measured by fluid displacement of the dissected lesion.

E. Statistical analysis of thermal lesion volume

Statistically significant differences of the lesion volume between experimental groups were determined using a two tailed, paired, Student's *t*-test. In the phantom study, lesion volume was measured as a function of exposure time and droplet concentration. For each condition, at least 5 lesions were formed to calculate the mean and standard deviation. In the *in vivo* liver study, MRI was used to measure the lesion volume. At least 3 lesions were generated at the same condition.

Results

A. In vitro phantom study

Visual- and MRI-measured thermal lesion volumes, formed with 4 s HIFU exposures and different droplet concentrations, are compared in Table 1. MRI volumetric measurements of the lesions were not statistically different from visual measurements ($p = 0.35$, two tailed

paired Student t-test), with a volume ratio of 0.98 ± 0.14 (MRI volume : visual volume). Another illustration of a very good agreement obtained between visual and MRI characterization of the lesions is given in Figure 4, in which images of lesions formed with droplet concentrations of 0, 10^4, and 10^5 droplets/mL for a 5 s HIFU exposure are present.

Steady increase in lesion size was observed as a function of exposure duration in phantoms at droplet concentrations of 0, 3×10^4, 9×10^4 and 3×10^5 droplets/mL, respectively. For a fixed exposure duration, larger lesions were seen with than without droplets (Figure 5). For a 5 s exposure, the average lesion volume was 7-fold larger in gels containing droplets at a concentration of 3×10^5 droplets/mL as compared to gels without droplets. For a 2 s exposure time, all lesions were less than 0.005 cm^3 in phantoms without droplets (n = 8). In contrast, in phantoms with droplet concentrations of 3×10^4 droplets/mL, 9×10^4 droplets/mL, and 3×10^5 droplets/mL lesions were 0.055 ± 0.007 cm^3, 0.075 ± 0.013 cm^3, and 0.083 ± 0.021 cm^3, respectively. Furthermore, the mean volume of lesions created with a 2 s HIFU exposure in droplet-containing phantoms was comparable (p = 0.96, two tailed paired Student t-test) to the lesion volume made in 5 s in phantoms without droplets (Figure 5).

For a fixed HIFU exposure time, the size of the HIFU lesions increased with droplet concentrations up to 10^6 droplets/mL. At a concentration of 10^6 droplets/mL, copious ADV bubbles were observed, but no lesions were detected by either visible, macroscopic imaging or MRI (Table 1), most likely because the two processes – ADV and HIFU occurred on different time scales, with ADV occurring on a much shorter time scale. As a result we hypothesize that the backscatter from the high-density ADV bubbles advanced the droplet vaporization proximally to shadow the focus, thus preventing the formation of a HIFU lesion. This assumption was confirmed by temperature measurements. In the 10^6 droplets/mL phantoms, temperature monitored 2 mm away from the focus by the thermocouple was consistently found to be 50 ± 5°C, *i.e.* lower than the protein denaturation temperature threshold of 60°C; whereas temperature measured in the 10^5 droplets/mL phantoms was found to be 75 ± 3°C, *i.e.* sufficiently high to cause protein denaturation. For all droplet concentrations and exposure times, no heating effects or protein denaturation was observed visually or by MRI in the prefocal or postfocal ultrasound propagation pathway.

B-mode images of the bubble cloud generated in each lesion were acquired immediately after HIFU application and compared to corresponding macroscopic optical images of the lesion in the lateral-elevational and axial-elevational planes. B-mode ultrasound was found to slightly overestimate the area by 10% or less in all examined cases (n = 7). Figure 6 demonstrates that the lesion shapes obtained optically and with ultrasound are very similar.

B. *In vivo* liver study

In vivo lesion production was demonstrated in a canine liver before and after IV injection of droplets with a similar acoustic setup as used in the *in vitro* studies. The vital signs of the animal were stable throughout the experiment. Three-dimensional HIFU lesion distribution in the liver is illustrated in Figure 7a using the MRI image volume data set. The corresponding projection image (Figure 7b) illustrates the diameter of each lesion. Average lesion volumes measured by MRI with ADV (5 s exposure, n = 3) and without ADV (5 s exposure, n = 4) were 0.265 ± 0.005 cm^3 and 0.017 ± 0.006 cm^3, respectively, a 15-fold difference. Lesion volumes (5 s exposure, n = 3) made 30 min after droplet injection (0.235 ± 0.035 cm^3) were not statistically different (p = 0.18, two tailed paired Student t-test) from those made immediately after droplet injection. Note that one post-ADV lesion of each 5 s exposure group was a partial lesion produced at the edge of the liver. Hence, they were excluded from the volume estimation. Figure 8 demonstrates the lesion size without and with ADV in the liver. Ultrasonic imaging of ADV bubbles (Figure 8 right) compared well

with the size and shape of thermal lesions imaged by MRI and optical imaging (Figure 8 left and middle).

Discussion

One of the aims of this study was to demonstrate the feasibility of using ADV to enhance localized HIFU therapy in a controllable manner. *In vitro* thermo-sensitive phantoms were used followed by an *in vivo* liver study. Both the *in vitro* and *in vivo* results showed that the use of ADV consistently increased the size of the produced HIFU lesion. *In vitro* results also indicated that the thermal lesion size depended on the droplet concentration and ultrasound exposure time.

It has been reported that the presence of bubbles will enhance the heating during HIFU treatment, either due to the appearance of cavitation bubbles (19, 39), or due to the presence of UCA to trigger the enhancement effect (40). The cause of increased heating in the presence of bubbles has been hypothesized as viscous damping of non-inertially cavitating bubbles, absorption of high frequencies created from inertial cavitation, and/or an increase in acoustic path length due to scattering. Nonlinear bubble effects have been exploited to enhance the local heat deposition in phantoms and soft tissues (6, 41). Mechanisms for microbubble-assisted heating were presented, modeled, and estimated by Holt and Roy (39) which showed similar results to the earlier work of Lele (42), Hynynen (43) and Charke and ter Haar (44). Modeling estimates from Holt and Roy (39) demonstrated that the heat deposition from bubbles can explain the measured temperature rises quantitatively. The role of inertial cavitation in enhancing the heating rate has also been shown by Farny et al. (19). Since ADV bubbles tend to be large, we hypothesize that viscous heating is the primary mechanism, however, further investigation is required to test this hypothesis.

The findings from the phantom experiments in the presence of droplets (3×10^5 droplets/mL) showed that the HIFU lesion volume increased by at least a factor of 7 for constant treatment time, or treatment time decreased by a factor of 2.5 (5 s without droplets vs. 2 s with droplets at 3×10^5 droplets/mL) for constant final lesion volume. The qualitative relationship between these effects can be summarized by ADV-enhanced HIFU increasing the rate of lesion formation. Therefore, HIFU therapy, assisted by ADV, can be achieved with a much shorter treatment time and a correspondingly reduced total acoustic power. This should lead to reduced tissue heating in the propagation path, a current major limitation in treatment times, and our phantom experiments demonstrated no heating effects or protein denaturation in the prefocal or postfocal ultrasound propagation pathway. In addition, the ADV microbubbles can block sound propagation beyond them (30), protecting distal tissues. During conventional HIFU therapy, for instance, tissues near the liver may preferentially heat, causing unintended pain and tissue damage. Periosteal pain is another example, which can be severe and is a challenge because of the rapid heat deposition of ultrasound in the bone (45, 46). Large gaseous boundaries, such as the diaphragm, lung, and bowel, as well as scar tissues and the umbilicus may heat at an accelerated rate relative to bulk soft tissue (47). In our *in vivo* liver study, no bleeding or extended tissue damage was observed. However, for these initial experiments, the liver was externalized during the experiment. Therefore, further chronic transcutaneous studies are warranted to evaluate the potential complications induced by HIFU ablation without and with ADV.

It is possible to create distal bubble barriers using ADV prior to the treatment as an additional layer of protection for sensitive tissues (30). These barriers may also be created using low duty cycle, microsecond pulses that will not generate thermal lesions. Hence, the treated volume may be well controlled, and the limitation of treating a large tumor volume will only be the long-term ability of the body to adjust to the necrotic volume or to tolerate

the treatment time. For the treatment of a large zone, we hypothesize that the ADV-enhanced HIFU will require less targeting sites to create a compound lesion throughout a predetermined volume, because the size of the individual lesions will be increased. Therefore, an increase in the maximum depth of treatment and in the number of treatable regions of restricted aperture should be realizable.

The stable vital signs of the canine during the experiment and the normal-looking lungs observed after the experiment implied minimal acute, unintended, bioeffects from the injected perfluoropentane droplets (36, 48, 49). However, a more thorough examination of potential bioeffects is warranted. It is noted that the volume increase of individual lesions was even larger in the canine liver with ADV (15×) as compared to those in the phantoms (7×), implying a substantially faster treatment of liver tissue than demonstrated earlier in the gel phantom. This effect may be due to the higher attenuation of liver for additional absorption or vascular trapping of these large bubbles from micron-sized droplets causing flow reduction or vascular occlusion. In future studies, thermal coagulative necrosis could be histologically evaluated using hematoxylin and eosin (H&E) staining and nicotinamide adenine dinucleotide (NADH) staining (50, 51).

The potential range and importance of successful thermal ablation with image-guided HIFU is growing rapidly. Its reduced cost or improved performance is described in various applications as either disruptive to existing medical approaches, as creating new treatment capabilities, or as synergistic with existing treatments (52). Ultrasound has advantages in its real-time guidance, wide availability, and cost effectiveness (53, 54). In this study, ultrasonic imaging of ADV bubble clouds was recorded as an independent measurement to MRI and visual measurement. Good agreement of the lesion size (Figure 8) was found between ultrasound and visual measurements, which implies that the controllable bubble clouds may be correlated to thermal coagulative necrosis. However, the B-mode ultrasound consistently overestimated the treated area by as much as 10%. The pressure threshold difference and the temporal difference between the ADV process and HIFU ablation may contribute to the overestimation. The ADV threshold at 1.44 MHz is approximately 5 MPa (26), which is lower than the thermal threshold of 7 MPa. Therefore, the amplitude required to form a HIFU lesion is higher than that for ADV. Additionally, the ADV process occurs on the order of microseconds (55), generating local gas bubbles much earlier than the formation of HIFU lesion. In comparison, one study showed that the MRI thermometry had led to an overestimation of thermal lesion diameter by as much as 40% although a very good correlation was found between the thermal dose and the MRI post-ablation image (56). Other MRI thermometry studies also compared thermal dose and the final lesion size, but showed controversial results with no statistically significant correlation (57). Our further investigation will focus on the consistency and predictability of the ultrasound imaging of the bubble clouds for volume estimation.

In the *in vivo* study, the liver is more echogenic when imaged with ultrasound than the tissue-mimicking phantom, which reduces the contrast between the bubble clouds and the background liver tissue. One solution is to subtract the two B-mode images taken before and after treatment. Alternatively, nonlinear ultrasound imaging, such as harmonic or subharmonic imaging, may increase the bubble-to-tissue contrast. The effects of threshold settings and imaging parameters will necessitate more investigation to determine a closer approximation of the acute lesion size on US. Various strategies for lesion detection using image processing may be applied to enhance the edge detection. As a result, image feedback via monitoring of ADV bubbles with ultrasound may aid in following the progression of lesion formation during treatment.

In summary, ADV substantially increased thermal lesion volumes by factors of 7 and 15 in gel phantoms and *in vivo*, respectively. Our results demonstrate that the size, shape, and location of the ADV bubble clouds in a B-mode ultrasound image may be predictive of those of the thermal lesion, which potentially provides a real-time, cost-effective feedback for image-guided therapy. Large individual lesions would imply a considerably faster treatment of tissue with compound lesioning. ADV, therefore, may have significant impact on the clinical implementation of HIFU.

Acknowledgments

This study was supported in part by NIH Grant No. 5RO1EB000281.

References

1. Boyle, P.; Levin, B., editors. World Cancer Report 2008. Lyon, France: IARC Press; 2008. p. 350
2. Yamasaki S, Hasegawa H, Makuuchi M, Takayama T, Kosuge T, Shimada K. Choice of treatments for small hepatocellular carcinoma: hepatectomy, embolization or ethanol injection. J Gastroenterol Hepatol. 1991; 6(4):408–13. [PubMed: 1655100]
3. Molinari M, Helton S. Hepatic resection versus radiofrequency ablation for hepatocellular carcinoma in cirrhotic individuals not candidates for liver transplantation: a Markov model decision analysis. Am J Surg. 2009; 198(3):396–406. [PubMed: 19520354]
4. Cancer Facts and Figures. American Cancer Society; 2004.
5. Hill CR, ter Haar GR. Review article: high intensity focused ultrasound--potential for cancer treatment. Br J Radiol. 1995; 68(816):1296–303. [PubMed: 8777589]
6. Coussios CC, Roy RA. Applications of Acoustics and Cavitation to Noninvasive Therapy and Drug Delivery. Annu Rev Fluid Mech. 2008; 40:395–420.
7. Lynn JG, Zwemer RL, Chick AJ, Miller AG. A new method for the generation and use of focused ultrasound in experimental biology. J Gen Physiol. 1942; 26:179–93. [PubMed: 19873337]
8. Burov AK. High-intensity ultrasonic vibrations for action on animal and human malignant tumours. Dokl Akad Nauk SSSR. 1956; 106:239–41.
9. Bamber JC, Hill CR. Ultrasonic attenuation and propagation speed in mammalian tissues as a function of temperature. Ultrasound Med Biol. 1979; 5:149–57. [PubMed: 505616]
10. Parker KJ. Ultrasonic attenuation and absorption in liver tissue. Ultrasound Med Biol. 1983; 9(4): 363–9. [PubMed: 6649154]
11. Frizzell LA. Threshold dosages for damage to mammalian liver by high-intensity focused ultrasound. IEEE Trans Ultrason Ferroelectr Freq Control. 1988; 35:578–81. [PubMed: 18290190]
12. ter Haar G, Sinnett D, Rivens I. High intensity focused ultrasound--a surgical technique for the treatment of discrete liver tumours. Phys Med Biol. 1989; 34(11):1743–50. [PubMed: 2685839]
13. ter Haar G, Coussios C. High intensity focused ultrasound: Physical principles and devices. Int J Hyperthermia. 2007; 23(2):89–104. [PubMed: 17578335]
14. Billard BE, Hynynen K, Roemer RB. Effects of physical parameters on high temperature ultrasound hyperthermia. Ultrasound Med Biol. 1990; 16(4):409–20. [PubMed: 2396329]
15. Zelkovic PF, Resnick MI. Renal radiofrequency ablation: clinical status 2003. Curr Opin Urol. 2003; 13(3):199–202. [PubMed: 12692441]
16. Chavrier F, Chapelon JY, Gelet A, Cathignol D. Modeling of high-intensity focused ultrasound-induced lesions in the presence of cavitation bubbles. J Acoust Soc Am. 2000; 108(1):432–40. [PubMed: 10923905]
17. Rabkin BA, Zderic V, Vaezy S. Hyperecho in ultrasound images of HIFU therapy: involvement of cavitation. Ultrasound Med Biol. 2005; 31(7):947–56. [PubMed: 15972200]
18. Coussios CC, Farny CH, Haar GT, Roy RA. Role of acoustic cavitation in the delivery and monitoring of cancer treatment by high-intensity focused ultrasound (HIFU). Int J Hyperthermia. 2007; 23(2):105–20. [PubMed: 17578336]

19. Farny CH, Glynn Holt R, Roy RA. The correlation between bubble-enhanced HIFU heating and cavitation power. IEEE Trans Biomed Eng. 2010; 57(1):175–84. [PubMed: 19651548]
20. Canney MS, Khokhlova VA, Bessonova OV, Bailey MR, Crum LA. Shock-induced heating and millisecond boiling in gels and tissue due to high intensity focused ultrasound. Ultrasound Med Biol. 2010; 36(2):250–67. [PubMed: 20018433]
21. Yang X, Roy RA, Holt RG. Bubble dynamics and size distributions during focused ultrasound insonation. J Acoust Soc Am. 2004; 116(6):3423–31. [PubMed: 15658693]
22. Stride EP, Coussios CC. Cavitation and contrast: the use of bubbles in ultrasound imaging and therapy. Proc Inst Mech Eng H. 224(2):171–91. [PubMed: 20349814]
23. Zhang S, Wan M, Zhong H, et al. Dynamic changes of integrated backscatter, attenuation coefficient and bubble activities during high-intensity focused ultrasound (HIFU) treatment. Ultrasound Med Biol. 2009; 35(11):1828–44. [PubMed: 19716225]
24. Umemura S, Kawabata K, Sasaki K. In vivo acceleration of ultrasonic tissue heating by microbubble agent. IEEE Trans Ultrason Ferroelectr Freq Control. 2005; 52(10):1690–8. [PubMed: 16382620]
25. Tung YS, Liu HL, Wu CC, Ju KC, Chen WS, Lin WL. Contrast-agent-enhanced ultrasound thermal ablation. Ultrasound Med Biol. 2006; 32(7):1103–10. [PubMed: 16829324]
26. Kripfgans OD, Fowlkes JB, Miller DL, Eldevik OP, Carson PL. Acoustic droplet vaporization for therapeutic and diagnostic applications. Ultrasound Med Biol. 2000; 26(7):1177–89. [PubMed: 11053753]
27. Rapoport N, Gao ZG, Kennedy A. Multifunctional nanoparticles for combining ultrasonic tumor imaging and targeted chemotherapy. Journal of the National Cancer Institute. 2007; 99(14):1095–106. [PubMed: 17623798]
28. Kawabata K, Sugita N, Yoshikawa H, Azuma T, Umemura S. Nanoparticles with multiple perfluorocarbons for controllable ultrasonically induced phase shifting. Japanese Journal of Applied Physics Part 1-Regular Papers Brief Communications & Review Papers. 2005; 44(6B): 4548–52.
29. Kripfgans OD, Orifici CM, Carson PL, Ives K, Eldevik OP, Fowlkes JB. Acoustic droplet vaporization for temporal and spatial control of tissue occlusion: a kidney study. IEEE Trans Ultras Ferroel Freq Control. 2005; 52(7):1101–10.
30. Lo AH, Kripfgans OD, Carson PL, Fowlkes JB. Spatial control of gas bubbles and their effects on acoustic fields. Ultrasound Med Biol. 2006; 32(1):95–106. [PubMed: 16364801]
31. Zhang M, Fabiilli ML, Haworth KJ, et al. Initial Investigation of Acoustic Droplet Vaporization for Occlusion in Canine Kidney. Ultrasound Med Biol. 2010 in press.
32. Kripfgans, OD. Book Acoustic droplet vaporization for diagnostic and therapeutic applications. University of Michigan; 2002. Acoustic droplet vaporization for diagnostic and therapeutic applications. City
33. Zhang P, Porter T. An in vitro study of a phase-shift nanoemulsion: a potential nucleation agent for bubble-enhanced HIFU tumor ablation. Ultrasound Med Biol. 2010; 36(11):1856–66. [PubMed: 20888685]
34. Fabiilli ML, Haworth KJ, Fakhri NH, Kripfgans OD, Carson PL, Fowlkes JB. The role of inertial cavitation in acoustic droplet vaporization. IEEE Trans Ultrason Ferroelectr Freq Control. 2009; 56(5):1006–17. [PubMed: 19473917]
35. Takegami K, Kaneko Y, Watanabe T, Maruyama T, Matsumoto Y, Nagawa H. Polyacrylamide gel containing egg white as new model for irradiation experiments using focused ultrasound. Ultrasound Med Biol. 2004; 30(10):1419–22. [PubMed: 15582242]
36. Flaim SF. Pharmacokinetics and side effects of perfluorocarbon-based blood substitutes. Art Cells, Blood Subs, and Immob Biotech. 1994; 22:1043–54.
37. Lambelet P, Ducret F, Leuba JL, Geoffroy M. Low-field nuclear magnetic resonance relaxation study of the thermal denaturation of transferrins. J Agric Food Chem. 1991; 39(2):287–92.
38. Weld KJ, Landman J. Comparison of cryoablation, radiofrequency ablation and high-intensity focused ultrasound for treating small renal tumours. BJU Int. 2005; 96(9):1224–9. [PubMed: 16287435]

39. Holt RG, Roy RA. Measurements of bubble-enhanced heating from focused, MHz-frequency ultrasound in a tissue-mimicking material. Ultrasound Med Biol. 2001; 27(10):1399–412. [PubMed: 11731053]
40. Lafon C, Murillo-Rincon A, Goldenstedt C, et al. Feasibility of using ultrasound contrast agents to increase the size of thermal lesions induced by non-focused transducers: in vitro demonstration in tissue mimicking phantom. Ultrasonics. 2009; 49(2):172–8. [PubMed: 18796342]
41. Yang X, Roy RA, Holt RG. Bubble dynamics and size distributions during focused ultrasound insonation. J Acoust Soc Am. 2004; 116(6):3423–31. [PubMed: 15658693]
42. Lele, PP. Effects of ultrasound on “solid” mammalian tissues and tumors in vivo. In: Repacholi, MH.; Grondolfo, M.; Rindi, A., editors. Ultrasound: Medical applications, biological effects and hazard potential. New York: Plenum Pub Corp; 1987. p. 273-306.
43. Hynynen K. The threshold for thermally significant cavitation in dog's thigh muscle in vivo. Ultrasound Med Biol. 1991; 17(2):157–69. [PubMed: 2053212]
44. Clarke RL, ter Haar GR. Temperature rise recorded during lesion formation by high-intensity focused ultrasound. Ultrasound Med Biol. 1997; 23(2):299–306. [PubMed: 9140186]
45. NCRP. Part 1: Exposure based on thermal mechanisms. Bethesda: National Council on Radiation Protection and Measurements; 1992. Exposure criteria for medical ultrasound.
46. Wootton JH, Ross AB, Diederich CJ. Prostate thermal therapy with high intensity transurethral ultrasound: the impact of pelvic bone heating on treatment delivery. Int J Hyperthermia. 2007; 23(8):609–22. [PubMed: 18097849]
47. NCRP-Comm-66. Book NCRP Report No 140. Exposure criteria for medical diagnostic ultrasound: II. Criteria based on all known mechanisms. National Council on Radiation Protection and Measurements; 2002. NCRP Report No 140. Exposure criteria for medical diagnostic ultrasound: II. Criteria based on all known mechanisms. City
48. Clark LC, Hoffmann RE, Davis SL. Response of the rabbit lung as a criterion of safety for fluorocarbon breathing and blood substitutes. Biomat, Art Cells & Immob Biotech. 1992; 20:1085–99.
49. Schutt E, Barber P, Fields T, et al. Proposed mechanism of pulmonary gas trapping (PGT) following intravenous perfluorocarbon emulsion administration. Art Cells, Blood Subs, and Immob Biotech. 1994; 22:1205–14.
50. Gettman MT, Lotan Y, Corwin TS, et al. Radiofrequency coagulation of renal parenchyma: Comparison of effects of energy generators on treatment efficacy. J Endourology. 2002; 16(2):83–8.
51. Klingler HC, Susani M, Seip R, Mauermann J, Sanghvi NT, Marberger MJ. A novel approach to energy ablative therapy of small renal tumors: Laparoscopic high-intensity focused ultrasound. European Urology. 2008; 53:810–8. [PubMed: 18069120]
52. Bradley WG Jr. MR-guided focused ultrasound: a potentially disruptive technology. J Am Coll Radiol. 2009; 6(7):510–3. [PubMed: 19560068]
53. Paskalev K, Feigenberg S, Jacob R, et al. Target localization for post-prostatectomy patients using CT and ultrasound image guidance. Journal of applied clinical medical physics [electronic resource] / American College of Medical Physics. 2005; 6(4):40–9.
54. Jaffray D, Kupelian P, Djemil T, Macklis RM. Review of image-guided radiation therapy. Expert Rev Anticancer Ther. 2007; 7(1):89–103. [PubMed: 17187523]
55. Kripfgans OD, Fabiilli ML, Carson PL, Fowlkes JB. On the acoustic vaporization of micrometer-sized droplets. J Acoust Soc Am. 2004; 116(1):272–81. [PubMed: 15295987]
56. Kohler MO, Mougenot C, Quesson B, et al. Volumetric HIFU ablation under 3D guidance of rapid MRI thermometry. Med Phys. 2009; 36(8):3521–35. [PubMed: 19746786]
57. Terraz S, Cernicanu A, Lepetit-Coiffe M, et al. Radiofrequency ablation of small liver malignancies under magnetic resonance guidance: progress in targeting and preliminary observations with temperature monitoring. Eur Radiol. 20(4):886–97. [PubMed: 19760231]

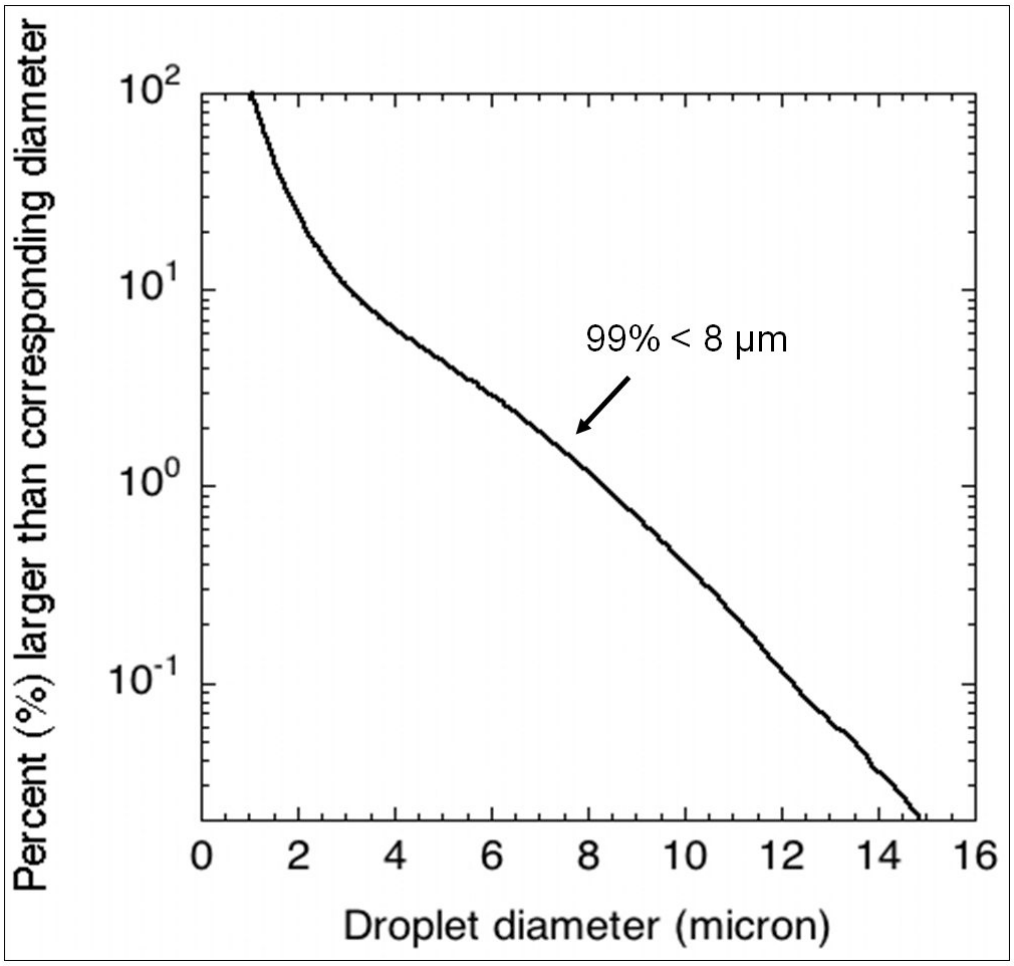

Figure 1.
Size distribution of the perfluoropentane droplets.

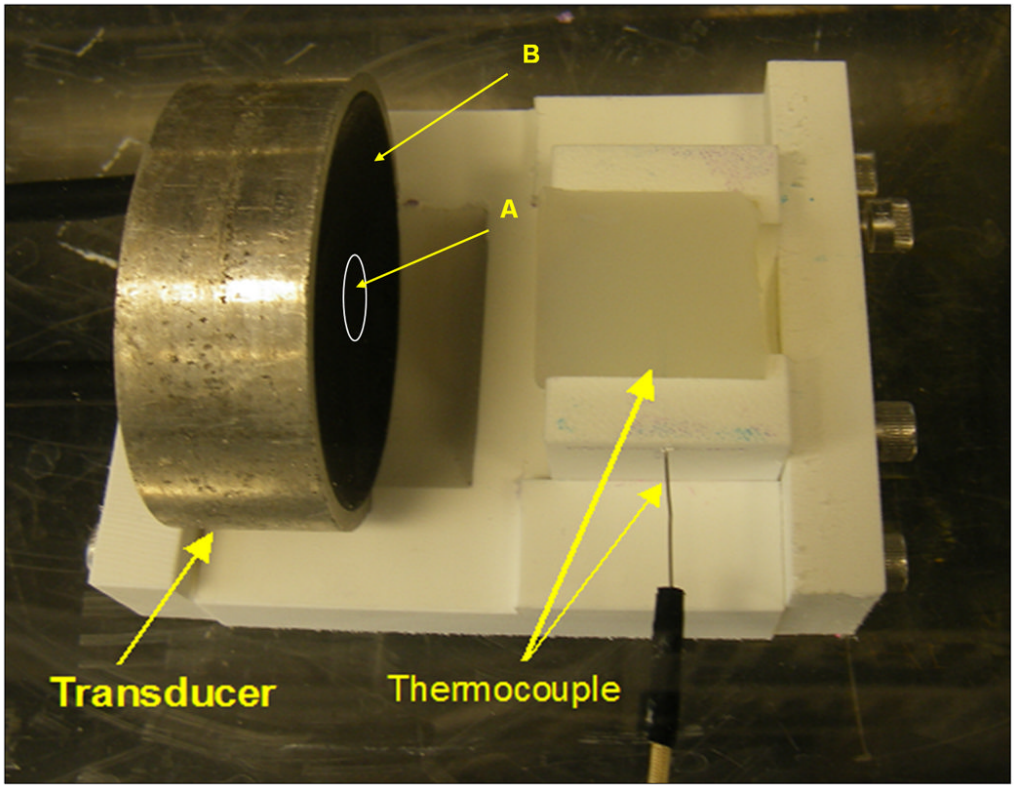

Figure 2.
Experimental setup of HIFU. The spherical section transducer is comprised of a center "imaging" element (A) surrounded by the annular "therapy" element (B). In this study, only the "therapy" element was used to generate thermal lesions. A cylindrical phantom (30 mm in diameter and 30 mm in length) is facing the transducer, and a HIFU lesion is generated at the depth of 15 mm in the phantom. A needle-type thermocouple enters the phantom from the side with the tip 2 mm away from the transducer focus.

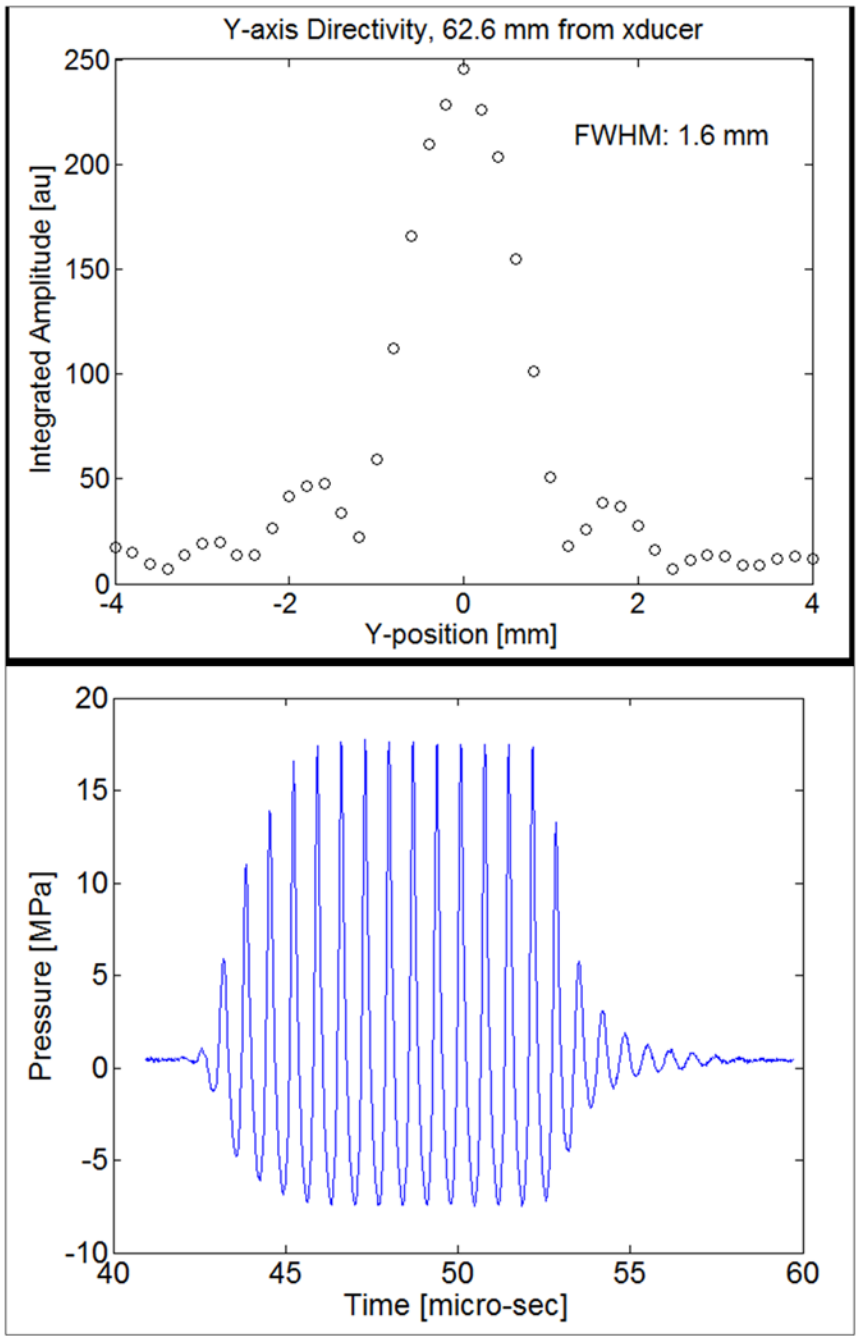

Figure 3.
The lateral beam profile at the focus of the therapy transducer (a) and the waveform acquired by the hydrophone (b).

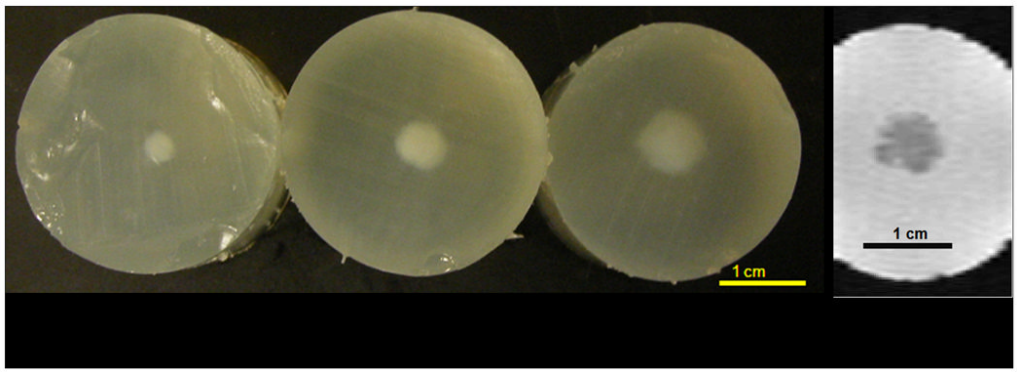

Figure 4.

Visible, macroscopic image (a) of cross-sections of HIFU lesions generated by 5 s of ultrasound exposure. In the macroscopic image, an impressive increase in lesion size is observed with droplets in concentrations of 0, 10^4, and 10^5 droplets/mL (from left to right). The MRI image (b) of the lesion with a droplet concentration of 10^5 droplets/mL is in good agreement with the macroscopic finding (phantom on the right). The denatured and cross-linked proteins in the lesion provide a significant decrease the water proton mobility and thereby a decrease in water proton T_2.

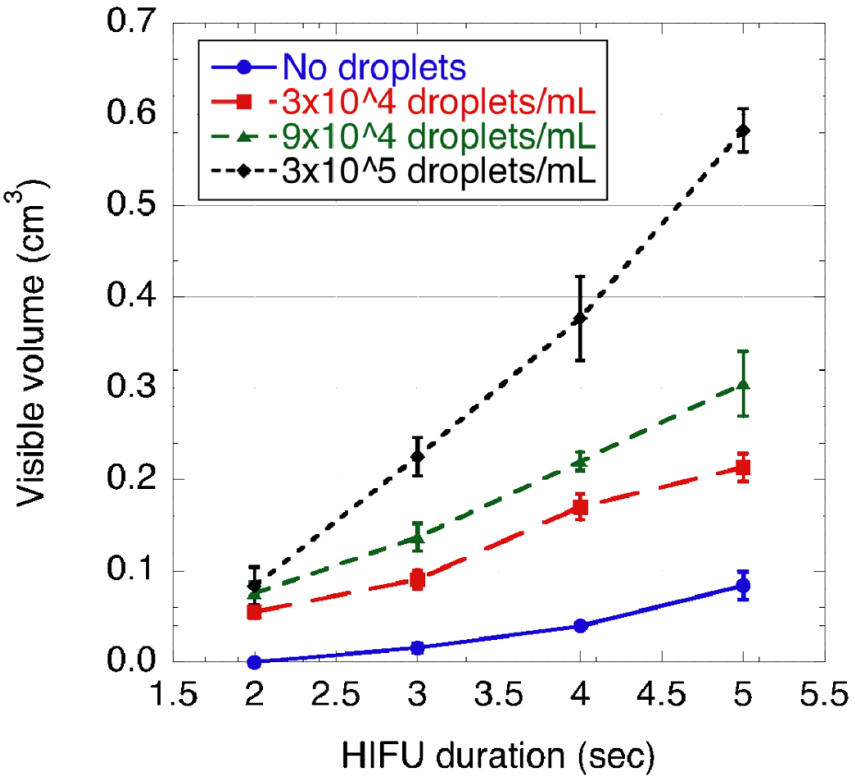

Figure 5.
Visible lesion volumes versus HIFU exposure duration. Each point corresponds to the average of the visible volume measured on 5 to 8 specimens at fixed experimental conditions.

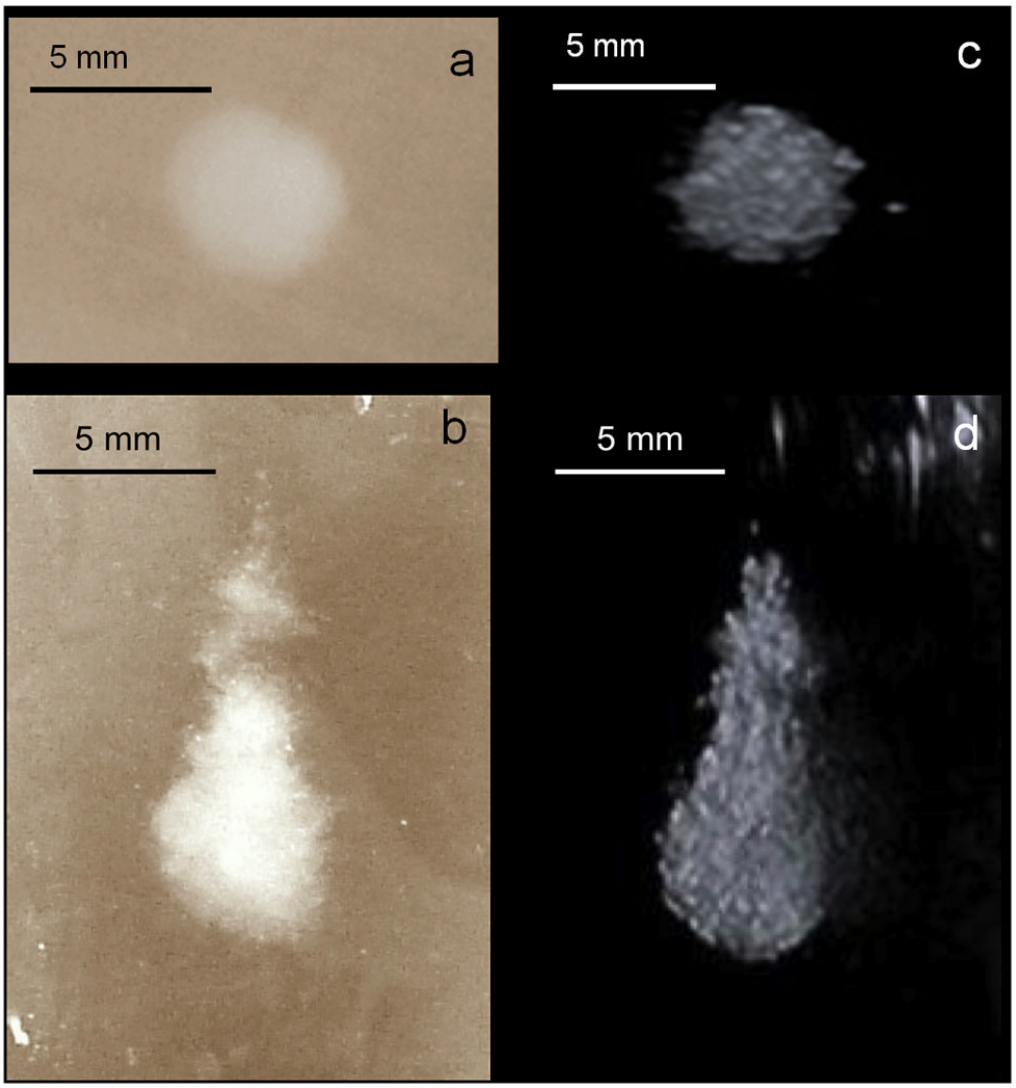

Figure 6.
Visible, macroscopic images (a and b) and B-mode images (c and d) of the same HIFU lesion. The top two images are in the lateral-elevational plane and the bottom two are in the axial-elevational plane. The therapy transducer and the imager were faced up towards the B-mode image (d).

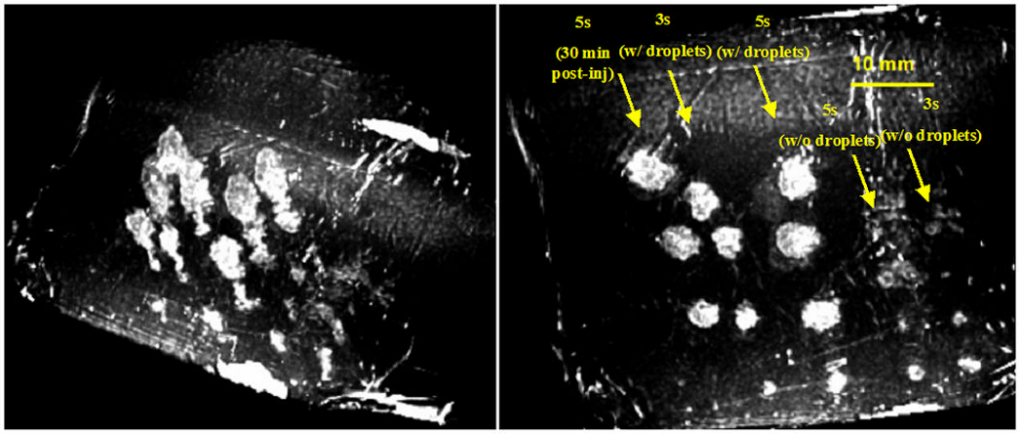

Figure 7.

Images displayed by thresholding the MRI data. 3D image of the layout of the HIFU lesions in the liver (a) and a corresponding projection image (b) indicating the diameters of these lesions (bar = 10 mm). The lesions at the bottom of the image, generated after ADV, were partial lesions formed at the thin edge of the liver. Therefore, they were excluded from the volume estimation.

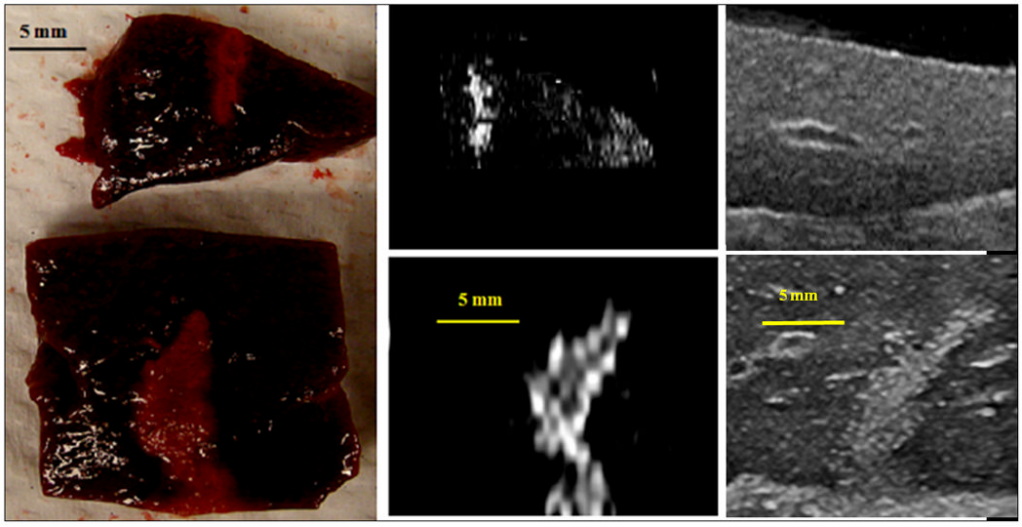

Figure 8.
Comparison of macroscopic, T_2-weighted MR and ultrasound images (left to right) of 5 s lesions without (top) and with (bottom) ADV. The shape and size of the lesion in these images are comparable indicating ultrasonic imaging of the bubbles may provide a guide for the HIFU treatment (bar = 5 mm).

Table 1

Comparison of lesion volume measured by MRI and visible macroscopic imaging with 4 s of HIFU exposure. It is noted that at the concentration of 10^6 droplets/mL, copious ADV bubbles were observed, but no lesions were detected by either visible, macroscopic imaging or MRI, possibly due to the backscatter from the high-density ADV bubbles advancing the droplet vaporization proximally to shadow the focus.

Droplet concentration (/mL)	MRI volume (cm^3)	Optical volume (cm^3)
0 (n=8)	0.05 ± 0.01	0.04 ± 0.01
10^4 (n=5)	0.10 ± 0.01	0.12 ± 0.02
10^5 (n=8)	0.29 ± 0.05	0.30 ± 0.05
10^6 (n = 8)	No lesion	No lesion